Backbone Dynamics of Rusticyanin: The High Hydrophobicity and Rigidity of This Blue Copper Protein Is Responsible for Its Thermodynamic Properties†

Beatriz Jiménez,‡ Mario Piccioli,§ José-María Moratal,‡ and Antonio Donaire*,‖

Departamento de Química Inorgánica, Universitat de València, C/ Dr. Moliner, 50, 46100-Burjassot (Valencia), Spain, Department of Chemistry and CERM, University of Florence, Via L. Sacconi, 6, 50019-Sesto Fiorentino (Florence), Italy, and Instituto de Biología Molecular y Celular, Universidad Miguel Hernández, Edificio Torregaitán, Avda. Ferrocarril s/n, 03202-Elche (Alicante), Spain

Received April 30, 2003; Revised Manuscript Received July 2, 2003

ABSTRACT: Local dynamics and solute−solvent exchange properties of rusticyanin (Rc) from *Thiobacillus ferrooxidans* have been studied by applying heteronuclear (^{1}H, ^{15}N) NMR spectroscopy. ^{15}N relaxation parameters have been determined for the reduced protein, and a model-free analysis has been applied. The high average value of the generalized order parameter, S^2 (0.93), indicates that Rc is very rigid. The analysis of cross correlation rates recorded in both the reduced and the oxidized forms conclusively proves that Rc possesses the same dynamic features in both oxidation states. The accessibility of backbone amide protons to the solvent at different time scales has also been studied by applying specific heteronuclear pulse sequences and by H_2O/D_2O exchange experiments. These experiments reveal that rusticyanin is extremely hydrophobic. The first N-35 amino acids, not present in the other BCPs, protect the β-barrel core from its interaction with the solvent, and thus, this is one of the main factors contributing to the hydrophobicity. Both characteristics (high rigidity and hydrophobicity) are maintained in the metal ion surroundings.

The thermodynamic properties of the blue copper protein (BCP)[1] rusticyanin (Rc) represent an intriguing issue in protein and copper biochemistries (*1*−*7*). BCPs are small soluble electron-transfer proteins containing a copper ion, which can be copper(I) or copper(II). All BCPs have a very rigid β-barrel structure that allows electron transfer to take place with a minimum reorganization energy (*1*). An extensive network of hydrogen bonds as well as tertiary interactions keep the tridimensional BCP structures. Rusticyanin can tolerate a wide range of pHs and is extremely stable at pH values lower than 2 (*8*−*10*). Rusticyanin is found in the Gram negative bacterium *Thiobacillus ferrooxidans* (*Tf*), where it constitutes the most abundant protein (ca. 6.5% of the weight of the soluble proteins in *Tf* corresponds to rusticyanin) (*11*, *12*). This organism extracts its energy by oxidizing iron(II) ions from the acidic environment in which it is found (*13*). Rc is probably the first acceptor in the electron transfer chain. The structural properties that provide Rc with its high stability over a wide pH range have been extensively analyzed by X-ray crystal diffraction (*14*−*19*), nuclear magnetic resonance (NMR) (*20*−*22*), and other spectroscopies (*23*−*25*), both in its native form and with different mutants (*19*, *26*). The fact that Rc possesses a β-barrel core that is more shielded from solvent in comparison with other BCPs has been proposed as one of the major factors determining these properties (*16*, *17*). Indeed, with 155 amino acids (it is the largest known BCP), Rc contains an N-terminal extension of 35 amino acids, not present in other BCPs. Recently, Hasnain et al. have studied the solution structure of a mutant with this N-35 extension deleted (N-35Rc) (*27*). This extension is directly implicated in keeping the high degree of hydrophobicity of the protein but not in its resistance to acidic media (*27*).

Rusticyanin also has an extremely high redox potential, which is found to be 300−500 mV higher than that of the other BCPs (*7*, *25*). Factors responsible for the extraordinary stabilization of the reduced form, Cu(I), in rusticyanin have also been discussed. Among these, the hydrophobicity of the active site (*16*, *22*, *28*) and the presence of a Ser at position 86 adjacent to the Cu ligand His85 (instead of an Asn, at the equivalent position in most other BCPs), which makes a hydrogen bond with the Sγ atom of the coordinated cysteine (*15*, *25*), are supposed to be particularly influential.

NMR is the technique that allows direct evidence on the dynamic range of the backbone mobility in proteins (*29*−*33*). It permits the characterization of the most mobile regions of a polypeptide chain as well as the time scale (pico-, nano-, or miliseconds) in which these movements occur. The degree of exposure to water molecules can also be determined by

† This work has been supported with financial aid from the DGICYT-Ministerio de Ciencia y Tecnología, Spain (BQU2002-02236, PB98-1444). The support from the European Large Scale Facility PARABIO at the University of Florence, Italy (Contract HPRI-CT-1999-00009) is acknowledged. B.J. and M.P. thank the Conselleria de Educación y Ciencia (Generalitat Valenciana) for a grant.

* Corresponding author. Phone: 34-96-6658942. Fax: 34-96-6658758. E-mail: adonaire@umh.es.

‡ Universitat de València.

§ University of Florence.

‖ Universidad Miguel Hernández.

[1] Abbreviations: Az, azurin; BCP, blue copper protein; ccr, cross correlation rates; NMR, nuclear magnetic resonance; NOE, nuclear Overhauser effect; Pc, plastocyanin; PsAz, pseudoazurin; Rc, rusticyanin; *Tf*, *Thiobacillus ferrooxidans*.

10.1021/bi034692q CCC: $25.00
Published on Web 08/13/2003

Table 1: Alignment of Secondary Structure Elements Present in Rc, Az, PsAz, and Pc. Residue Numbers Including These Elements Are Given for Each BCP

secondary structure element[a]	residue number in:			
	Rc[b]	Az[c]	PsAz[d]	Pc[e]
β-strand I[f]	*8−10*			
helix I[f]	*11−20*			
β-strand II[f]	*25−27*			
β-strand III[f]	*30−33*			
β-strand IV	36−45	3−10	2−8	1−6
β-strand V	53−57	14−16	17−19	13−15
β-strand VI[f]	*59−61*			
β-strand VII	63−66	18−22	22−25	17−21
β-strand VIII	71−79	27−36	30−34	26−33
loop(80−119)	80−119	37−90	35−63	34−66
		β-strand[h] *46−51*		*40−42*
ligand 1	His85	His46	His40	His37
		helix[h] *55−67*		
turn 93−97[g]	93−97	74−76	52−56	46−49
β-strand IX	120−127	91−98	64−67	67−74
		helix[h] 100−102		
β-strand X	132−138	108−112	72−78	78−84
ligand 2	Cys138	Cys112	Cys78	Cys84
ligand 3	His143	His117	His81	His 87
helix II[f]	*144−146*			
ligand 4	Met148	Met121	Met86	Met92
β-strand XI	148−155	121−128	86−92	92−99
			helix[i] 99−104	
			helix[i] *109−122*	

[a] The numeration of the secondary structure elements is given according to rusticyanin sequence. [b] *Tf* rusticyanin (*16*, *22*). [c] *P. aeruginosa* azurin (*40*). [d] *P. pantotrophus* pseudoazurin (*41*). [e] *Synechocystis* sp. PCC6803 plastocyanin (*42*). [f] These elements, written in italics, are unique of Rc (for the sake of clarity, they are located in the right side of the first column). [g] Turn 93−97 in Rc is aligned with regions described in Table 1 for the other BCPs on the basis of the similar mobility pattern (see text). [h] Elements only present in Az. [i] Elements exclusive of PsAz.

D_2O/H_2O exchange experiments. Moreover, NMR spectroscopy reveals the position of the solvent molecules buried inside the protein (*34−39*). Water−protein interactions studied by applying this technique provide important information on the degree of hydrophobicity of a protein, on the regions more exposed to the solvent, and on the time scale of such protein−water interactions. The knowledge of the dynamic properties of Rc and the recognition of the residues that interact with water molecules are important to identify the factors that provide Rc with its stability features at low pH values.

The dynamic behavior of three BCPs has been already determined: azurin (Az) from *Pseudomonas aeruginosa* (*40*), pseudoazurin (PsAz) from *Paracoccus pantotrophus* (*41*), and plastocyanin (Pc) from *Synechocystis* sp. PCC6803 (*42*). Like all BCPs, a β-barrel represents the main structural element for these proteins. Pc, the smallest BCP, presents the basic tertiary structures of these proteins. Additional secondary structural elements are present in some of them but not in others. For instance, the N-35 extension of Rc contains three β-strands and an α-helix not present in the rest of BCPs. For the sake of clarity, we report the residue alignment of Rc and these three BCPs in Table 1. The three cited BCPs (Az, PsAz, and Pc) are highly rigid and show a similar mobility pattern for equivalent regions of the proteins (*40−42*). Only Pc has been characterized in the two redox states of the copper ion, although no significant differences have been found between the dynamic properties of Cu(I) and Cu(II) plastocyanin (*42*).

We have tried here to relate the structural elements peculiar to Rc with its dynamic properties and to explain how internal mobility affects its unique thermodynamic features (i.e., stability at low pH and high redox potential).

EXPERIMENTAL PROCEDURES

NMR Sample Preparation. Rusticyanin labeled with ^{15}N or with ^{13}C and ^{15}N was obtained from cultures of *Escherichia coli* strains BL21(DE3) containing the rusticyanin plasmid (*10*). A slightly modified M9 minimum medium (Glucose 8.0 g/L, KH_2PO_4 20.0 g/L, Na_2HPO_4 18.2 g/L, NaCl 1.0 g/L, $^{15}NH_4Cl$ 1.0 g/L, $MgSO_4 \cdot 7H_2O$ 1 M solution 2 mL/L, and $CaCl_2$ 1 M solution 400 μL/L) was used. Ampicillin (concentration 200 mg/mL) was also added to the culture in a ratio of 1 mL/L. Two L of this medium was inoculated with 50 mL of *E. coli* cells and kept at 38 °C for 5 h. Then, 400 μL/L isopropyl-β-thiogalactopyranoside, IPTG, solution (200 mg/L) was added to induce protein expression. After ca. 20 h, the cells were collected. Labeled ^{15}N rusticyanin was obtained and purified as previously described (*10*). The yield typically was ca. 70 mg of protein/L of culture medium. Samples were then concentrated in H_2O, acetate buffer 100 mM, pH 5.5 with Biomax−5K NMWL membrane (15 mL) and centricons (3 mL) both from Millipore. For copper(I) rusticyanin measurements, metal reduction was achieved by adding small quantities of sodium dithionite. For the measurements performed in oxidized samples, an excess of sodium ferricyanide was added with the opposite aim. In both cases, the sample was washed to eliminate the excess of reducing or oxidizing agent, prior to NMR measurements.

For the H_2O/D_2O exchange experiments, a sample in H_2O (1.2 mM, acetate buffer 100 mM, pH 5.5) was washed against a D_2O solution at the same conditions in Millipore centricon devices, and the $^1H-^{15}N$ heteronuclear single quantum correlation (HSQC) spectra (*43*) of this freshly prepared sample was recorded (0 h). Then, HSQC experiments in analogous experimental conditions were recorded every hour during the first 8 h and then at increasing periods over 14 days.

NMR Measurements. NMR experiments were performed at 296 K both in a Bruker Avance 500 or in a Bruker Avance 600 spectrometer operating at magnetic fields of 11.7 and 14.1 T, respectively. ^1H and ^{15}N frequencies were, respectively, 500.13 (600.13) and 50.68 (60.81) MHz for a magnetic field of 11.7 (14.1) T. $^1H-^{15}N$ HSQC experiments (*43*) were recorded before and after each experiment to check the state of the sample. The assignment of the $^1H-^{15}N$ HSQC cross peaks was performed by comparison with data available in the literature (*20*). In the reduced state, a 3-D $^1H-^{15}N$ HSQC-TOCSY experiment (*44*) (with 50 ms of spin lock) was carried out to distinguish any ambiguities that may occur between the chemical shifts in our working conditions and the previously reported assignment. For the oxidized state (not previously assigned), the uncertainties were eliminated with an HNCA experiment (*45*, *46*) using a previous assignment of ^{13}C carbon resonances in the reduced state (*21*).

^{15}N longitudinal, R_1 (*31*), and transversal, R_2 (*31*, *47*), relaxation rates as well as $^1H-^{15}N$ NOE (*48*) values were

measured by using the pulse sequences previously reported on a Cu(I) Rc sample (3.0 mM, acetate buffer 100 mM, pH 5.5, 296 K). For R_1 measurements, eight experiments with ^{15}N recovery delays of 10, 60, 130, 150, 250, 290, 500, and 800 ms were performed. The relaxation delay after the acquisition time was 3 s. Another eight experiments with ^{15}N recovery delays of 6.9, 13.8, 27.6, 48.3, 75.9, 110.4, 151.8, and 207 ms during the transversal evolution of the ^{15}N nucleus were carried out to determine their R_2 values. Water suppression was achieved by an echo−antiecho scheme (*49*). For the determination of ^{1}H−^{15}N NOE values, three experiments with ^{1}H presaturation for 2.5 s and one without were performed. In this last case, the strong solvent signal was partially eliminated by a flip-back approach (*48*). For R_2 and ^{1}H−^{15}N NOE experiments, 3.2 s of recycle time was employed to ensure the complete nuclei relaxation.

Measurements of cross correlation rates occurring between ^{15}N chemical shift anisotropy (csa) and ^{15}N−^{1}H dipole−dipole relaxation were performed using the pulse sequence described by Tjandra et al. (*50*). The duration of the dephasing delays used were 23.4, 34, 48, and 66 ms. These experiments were taken both in a reduced and in an oxidized sample (acetate buffer 100 mM, pH 5.5, 296 K in both cases). Experiments to determine amide proton in exchange with the bulk solvent, ^{15}N-(CLEANEX-PM)-FHSQC (cleanex experiment, hereafter) (*51*), and with water molecules residing in the protein for a time longer than the correlation time (ePHOGSY) (*52*, *53*) have also been performed in a reduced sample (acetate buffer 100 mM, pH 5.5) by applying the previously reported pulse sequences.

In all heteronuclear ^{1}H−^{15}N HSQC experiments, 2048 × 220 data points were collected in the ^{1}H and ^{15}N dimensions, respectively. For relaxation and NOE measurements, spectral windows of 13.0 and 30.0 ppm for ^{1}H and ^{15}N nuclei were used. For cleanex and ePHOGSY experiments, the spectral windows were enlarged in both dimensions (25.0 and 100 ppm in ^{1}H and ^{15}N, respectively) to observe histidine imidazol Hϵ1 protons. The carrier signal was set to the H_2O signal in all cases. FIDs were apodized to a final data matrix of 2048 × 1024 points, zero filled, weighted with Gaussian and sine square (shifted 60°) functions in acquisition and evolution dimensions, respectively, and Fourier transformed. Only the downfield part of the ^{1}H spectra, containing the H−N connectivities, was kept for the data analysis. The cross peaks were integrated using the standard routine of the Bruker XWINNMR program.

Data Analysis. Relaxation rates, R_1 and R_2, were determined by fitting the cross peak intensities of the corresponding experiments to a single-exponential decay by using the Levenberg−Marquardt algorithm (*54*, *55*), according to the following expression: $I(t) = A + B\exp(-R_i t)$, where A, B, and R_i (with $i = 1$ or 2) are adjustable parameters. The parameter A was set to 0 for transversal relaxation, R_2, measurements. Uncertainties in R_1 and R_2 values were obtained by using a Monte Carlo approach (*56*, *57*).

The ^{1}H−^{15}N NOE values were obtained by the ratio between the intensity of each peak in the experiments with and without presaturation of the amide protons. Errors were taken as three times the standard deviation, σ, of the differences in the intensities of the three experiments performed with HN presaturation.

The analysis of the overall tumbling of Rc was performed from the R_2/R_1 ratios of each H−N pair by the program Quadric Diffusion 1.11 (*58*). The average structure (previously minimized) of the rusticyanin family of structures (1cur (*22*) from the Protein Data Bank, PDB) was used in these calculations. R_2/R_1 values larger than twice the standard deviation (σ) of the average value were eliminated (*59*). This process was repeated until all values fell within the average value $\pm 2\sigma$. Throughout this article, the same criterium has been taken for discerning among data that do and do not deviate from the average value. This has allowed us to discriminate H−N pairs with individual dynamic behavior from those with the same pattern as the overall protein frame. The diffusion parameters corresponding to isotropic, axially symmetric, and fully anisotropic models were tested (*57*, *60*). The F factor (*61*, *62*) was used to check the statistical improvement of the fitting to each model.

The relaxation data (R_1, R_2, and ^{1}H−^{15}N NOE) were analyzed according to the model-free approach of Lipari and Szabo (*63*, *64*), by using the program Modelfree 4.0 (*60*). The spectral density function, $J(\omega)$, is given by

$$J(\omega) = \frac{2}{5}\left[\frac{S^2\tau_r}{1+(\omega\tau_r)^2} + \frac{(1-S)^2\tau_c}{1+(\omega\tau_c)^2}\right] \quad (1)$$

where τ_r is the correlation time for the overall tumbling of the molecule; S^2 is the order parameter; and $\tau_c^{-1} = \tau_r^{-1} + \tau_e^{-1}$, in which τ_e is the correlation time for internal motions. The experimental data were adjusted into one of four different previously described models (*57*, *60*). In all the models, the order parameter, S^2, was always fitted. Model 1, with only a correlation time (the rotational time of the molecule, τ_r) is valid for H−N couples with no internal motions (i.e., within the movement of the whole protein frame) (only S^2 was fitted). Model 2 adds to the fitting a correlation time (τ_e) that accounts for fast (subnanosecond) internal motions. The fitting with model 3 only uses a total correlation time (τ_r), as model 1, but exchange phenomena in the micro-/millisecond time scale are accounted for by an exchange rate, R_{ex}, parameter. Model 4 is analogous to model 2 (includes a τ_e parameter) and to model 3 (also includes exchange, R_{ex}, phenomena). If the sum of squared errors (SSE) was lower than 10 for model 1, then this model was taken as correct for the corresponding H−N. For larger SSE values, models 2 or 3 were applied and assumed as correct if SSE < 10. Only for one residue (Leu46, see Results) was model 4 assumed.

Cross correlation rates (ccr) between ^{15}N and ^{1}H dipolar interaction and ^{15}N csa were obtained from the fitting of the expression: $I_A/I_B = \tanh(2\Delta\eta)$, where I_A and I_B are the intensities of a given peak for each evolution Δ delay in the two experiment schemes previously reported (*50*), and 2η are the ccr values. When no exchange phenomena are present, these ccr values are, in a good approximation, proportional to the generalized order parameter, S^2 (*50*).

RESULTS

Relaxation Data. From ^{15}N HSQC experiments, 137 out of the 140 backbone amide groups have been identified. The assignment of the signals was performed by comparison with that previously published (*20*). A 3-D ^{15}N HSQC-TOCSY

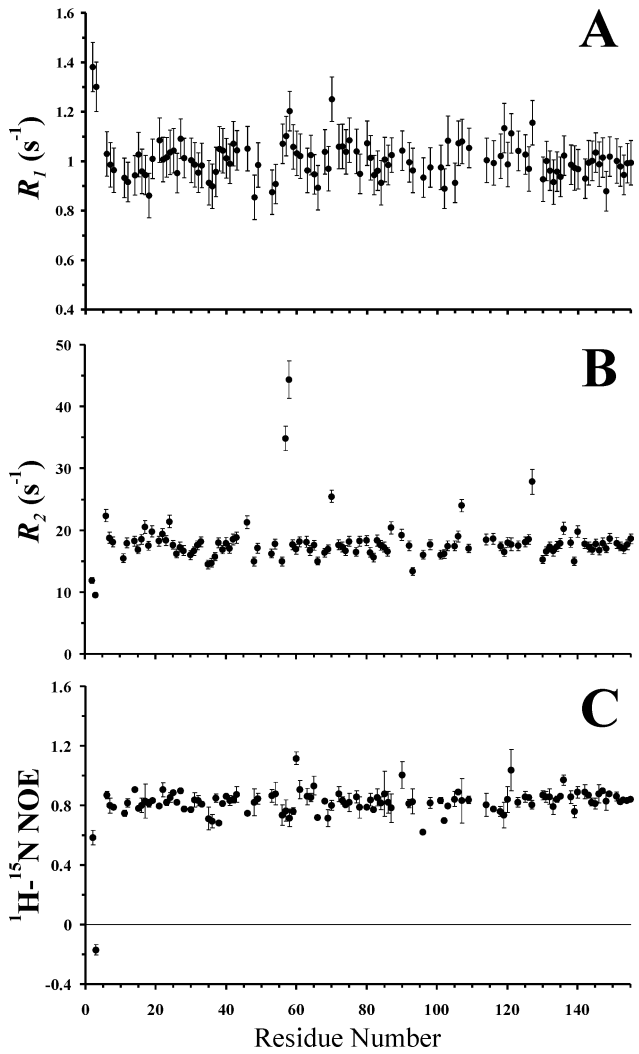

FIGURE 1: Relaxation data for the reduced rusticyanin (3.0 mM, acetate buffer 100 mM, pH 5.5, 296 K): (A) longitudinal relaxation rates (R_1); (B) transversal relaxation rates (R_2); and (C) ^{1}H−^{15}N NOE values.

experiment was used to check the validity of the assignment. As a consequence of different experimental (pH and temperature) conditions, about 30% of the signals change their chemical shifts. However, no inconsistency was found between both assignments. Twenty-six backbone amide peaks were either too weak or overlapped, therefore rendering a complete analysis of their relaxation properties unreliable. The whole body of the relaxation data obtained for 111 peaks is shown in Figure 1A−C.

The average value of the longitudinal relaxation rates (R_1) of the ^{15}N backbone nuclei was 1.00 ± 0.06 s^{-1}. Six residues (Thr2, Leu3, Asp58, Ala70, Lys119, Trp127) exhibit R_1 values larger than the average by more than 2σ, suggesting the occurrence of some internal motions. The average value of the transversal relaxation rates (R_2) was 17.4 ± 1.2 s^{-1}. Eight residues (Thr6, Gly24, Leu46, His57, Asp58, Ala70, Ala107, and Trp127) have R_2 values significantly larger than this average value. The pattern of Figure 1B clearly shows that the R_2 values in the region 57−58 are unambiguously above the general trend of the molecule. This is indicative of conformational exchange phenomena occurring on time scales longer than the nanosecond time, and thus, contributing to R_2 relaxation for these few residues (*31*, *60*). There are also some amino acids (Thr2, Leu3, Gly35, Lys36, and Gly93) with R_2 values below the average value (Figure 1B), thus indicating internal motions on the subnanosecond time scale. The average ratio for R_2/R_1 residues calculated for 97 residues (i.e., with those ones whose R_2/R_1 ratios do not exceed twice the standard deviation) is 17.6 ± 1.2. Given the small spread in R_1 values, the pattern of R_2/R_1 (data not shown) largely follows the behavior of Figure 1B, pointing out those residues that undergo conformational dynamics in the micro-/millisecond time scale.

Eleven residues (Thr2, Leu3, Gly35, Lys36, Val38, Val56, Asp58, Ile66, Gly69, Tyr96, and Ile102) have NOE values lower than twice the standard deviation of the medium NOE. Remarkably, Leu3 NOE is negative, indicating that the N-terminal residues are largely unstructured.

For some of the above amino acids, the occurrence of motional properties on the scale of the correlation time was already indicated by R_2 measurements. Apart from these residues, the average NOE value is 0.83 ± 0.04. This is very close to the maximum theoretical NOE value (0.835) expected in the case of a protein with no internal motions (*57*, *60*). The results, summarized in Figure 1C, show that four residues (Lys60, Glu65, Thr90, Gly121) deviate their NOE values from the average by more than 2σ. In the case of Lys60 and Gly121, which are solvent exposed, this is probably due to the existence of exchange phenomena between the amide protons and the solvent, which may affect the intensity of the signals of the reference experiment (*48*, *65*).

The experimental data, summarized in Figure 1, point out the presence of internal mobility in the N-terminal side of the molecule, in the region spanning amino acids 35−38, and in the regions encompassing the residues 56−58, 66−70, and 93−96. The nature of such internal motions and a more comprehensive understanding of their time scale and efficiency can be analyzed by a model-free analysis.

Model-Free Analysis. The inertia tensor calculated for the average NMR structure of Rc (1cur (*22*) from the PDB) has principal values in the ratio 1.00:0.80:0.71. The individual local correlation times estimated from the R_2/R_1 ratio for each residue were satisfactorily fitted by using the isotropic model. The effective correlation time, τ_r, for Rc was 13.2 ns. When axial and fully anisotropic models were considered, F test values of 3.08 and 0.6 were respectively obtained, indicating no statistically significant improvement of the fit with the increment of parameters. Therefore, all calculations were performed by assuming an isotropic model. The same diffusion model has been found for azurin (*40*), while an axially anisotropic one was used both for pseudoazurin (*41*) and for plastocyanin (*42*). The simple inspection of the tridimensional structures of these molecules can explain these results. In fact, both Pc and PsAz have close to cylindrical shapes. On the contrary, Rc and Az are more spherical.

The order parameter, S^2, was calculated for each residue by applying the model-free analysis (*57*, *60*) and according to the four dynamic models mentioned in Experimental Procedures. Figure 2A displays the S^2 values for the 111 residues whose relaxation properties have been determined. Following the procedure described in Experimental Procedures, an average of 0.93 ± 0.03 for the order parameter was obtained. The overall trend of the order parameter

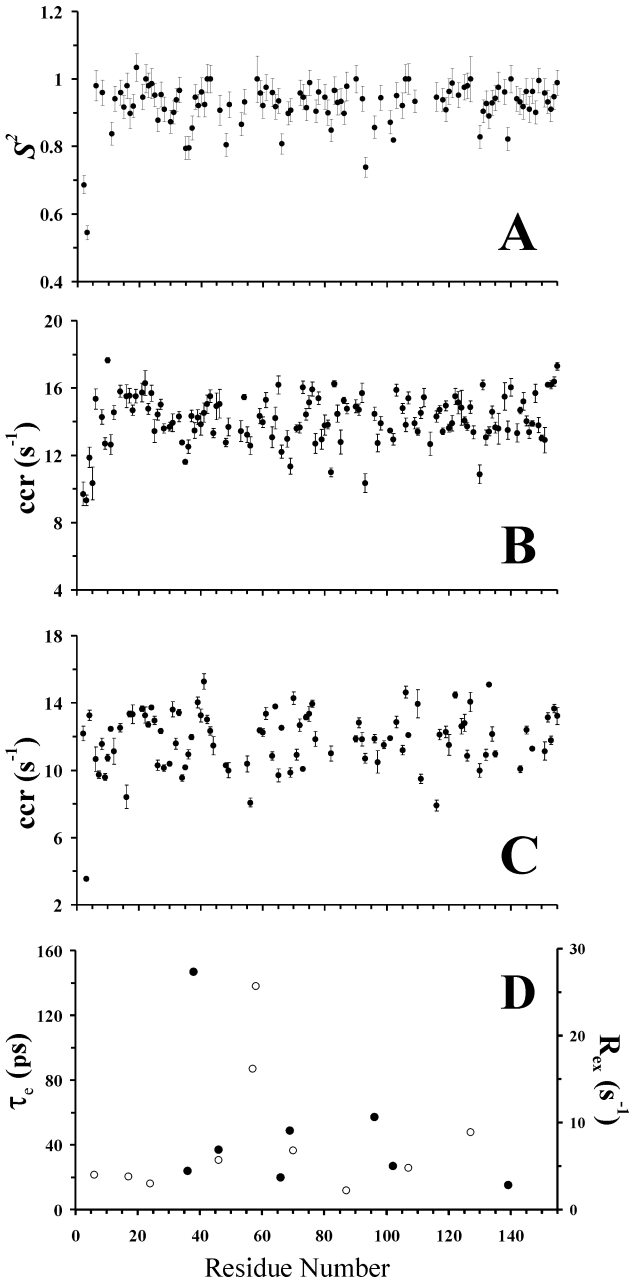

FIGURE 2: (A) Generalized order parameter, S^2, vs the residue number for the reduced Rc; (B) cross correlation rates for the reduced Rc; (C) cross correlation rates per residue for the oxidized Rc; and (D) correlation times (τ_e, plain dots, left *y*-axis) for residues with fast (subnanosecond) internal motions (these residues have been fitted according to models 2 or 4) and exchange rates (R_{ex}, open dots, right *y*-axis) for residues implicated in dynamics in the micro- or millisecond time scale (models 3 or 4).

reflects the secondary structure elements of the protein, with the highest values on the α-helix (0.93) and the β-strand (0.94) motifs and the largest flexibility in the short loop regions both in the northern and in the southern part of the β-barrel. Ten residues show an S^2 lower than twice the standard deviation: Thr2, Leu3, Gly35, Lys36, Gly48, Ile66, Gly93, Ile102, Thr130, and Gln139. The low values observed for residues 2−3 and 35−36 point out that the mobility of the N-terminus and the 35−37 region is higher than that of the rest of the molecule. The other residues are all located in loop regions. Additionally, they are either adjacent to (Gly48, Ile66, Gly93, and Thr130) or only two residues from (Ile102, Gln139) proline residues, which typically contribute to local mobility. The four copper bound residues have values spanning from 0.90 to 0.96 and are, therefore, perfectly on average with the mobility of the whole protein.

Ninety-four out of 111 amino acids (84.7%) fit within the model 1 of the model-free analysis. Seven residues (Lys36, Val38, Ile66, Gly69, Tyr96, Ile102, and Gln139) were fitted by taking into account fast internal motions on the subnanosecond time scale (model 2). Two of them, Lys36 and Val38, are located in a region that, on average, has clearly a higher mobility than the rest of the protein. Also, the value observed for Ile66 and Gly69 points out the occurrence of a region, roughly defined between β-strands VII and VIII, with less restricted motions. The same consideration also holds for Tyr96, which is (excluding the N-terminal amino acids) the residue with the lowest order parameter. Tyr96 is located in a Gly-Pro-Pro-Tyr stretch that, in turn, constitutes a part of the 40-residue loop 80−119 connecting strands VIII and IX. The correlation times (τ_e) observed for these residues, shown in Figure 2D, vary between 15 and 147 ps.

Nine residues (Thr6, Ala17, Gly24, Val56, His57, Asp58, Ala70, Ala107, and Trp127) are fitted only when an exchange time constant in the millisecond time scale is introduced (model 3). The model-free analysis also reveals the existence of conformational exchange phenomena (R_{ex}, Figure 2D) for these residues in time scales longer than the overall molecular tumbling. These exchange rates are in the 2.2−25.7 Hz range. While most of them are lower than 5 Hz, considered as a threshold for the detectability of conformational exchange effects (*66*), the region His57−Asp58, which corresponds to a tight loop between sheets V and VI, is unambiguously above that limit. Ala70 and Trp127 are also above this threshold. Finally, Leu46 is the only residue that fits according to model 4, with τ_e and K_{ex} values of 37 ps and 5.7 Hz, respectively.

Cross Correlation Rates. Reduced State. As already extensively shown in the literature, a quantitative analysis of cross correlation between $^{15}N-^{1}H$ dipolar interaction and ^{15}N chemical shift anisotropy (csa) is, within a 5−10%, a good marker of fast internal dynamics (*50*, *67*).

Cross correlation rates (ccr) were safely estimated for 127 out of the 140 NH backbone groups for a copper(I) Rc sample (3.0 mM, acetate buffer 100 mM, pH 5.5). The results, spanning from 17.6 (Ala10) to 9.3 (Leu3) s^{-1}, are shown in Figure 2B. As observed, ccr values follow closely the behavior of the S^2 parameters. Thus, both are complementary and consistent, as previously demonstrated in other proteins (*50*, *67*). The average ccr value was 14.1 ± 1.0 s^{-1}. Two regions, the first α-helix (amino acids 10−20, see Table 1) and the C-terminal β-strand (residues 148−155), display higher values than the average (14.9 and 15.2 s^{-1}, respectively). Residues Ala10 and Lys155, which belong to the above regions, possess the highest ccr values of the protein. Besides the amino acids of the N-terminal region, the lowest ccr values correspond to residues Gly35, Gly82, Gly93, and Thr130, belonging to different loops of the protein. With the exception of Gly82 (whose order parameter was not determined), model-free analysis for all these residues is in agreement with ccr data. The Gly82 ccr value suggests that this glycine experiences internal motions on the subnanosecond time scale.

Cross Correlation Rates. Oxidized State. Measurements of cross correlation rates were also performed on a Cu(II)

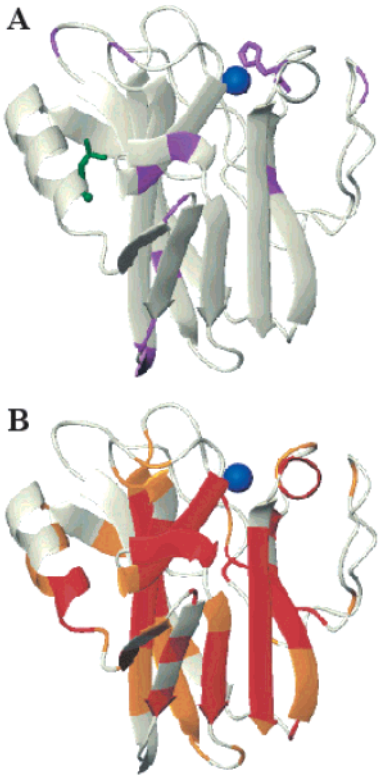

FIGURE 3: (A) Map of the Rc residues with fast exchangeable amide protons in magenta, obtained from the cleanex experiment (1.2 mM, acetate buffer 100 mM, pH 5.5, 296 K). The side chain of His143, with the very fast exchangeable NHϵ2 proton, is plotted as well. The structural water molecule detected in the ePHOGSY experiment (*52*, *53*) close to Leu19 (see text) is also plotted in green. (B) Schematic view of Rc backbone displaying the amide protons with fast (white), medium (orange), and slow (red) D_2O/H_2O exchange pattern (see text).

oxidized sample (2.2 mM, acetate buffer 100 mM, pH 5.5, Figure 2C). Comparison of ccr values in the reduced and oxidized states showed no significant deviation, except for some residues close to the metal center. This effect is due to the fast relaxation of the nuclei close to the paramagnetic center and is not related with the dynamics of the protein. This unambiguously shows that the mobility features of Rc are essentially independent of the oxidation state of the metal ion.

Water Exchange. The cleanex experiment (*51*) allows the detection of HN amide protons that exchange with the bulk solvent on the millisecond time scale. It enables the identification of those protein regions that are most accessible to the solvent. It appears that most of the residues in Rc are in a high hydrophobic environment, with low accessibility for water molecules. Only 10 residues (Gly28, Ser34, Lys36, Gly48, Val56, Lys60, Asp73, Ala97, Gly118, and Tyr136) are clearly observed in the cleanex experiment (see Supporting Information). Figure 3A displays the location of these residues in the protein architecture (residues in magenta). This pattern shows unambiguously that the region encompassing amino acids 28−36 is quite accessible to the solvent and therefore amenable to undergo exchange phenomena. An inspection of Rc structure shows that this region (which includes the β-strand III, see Table 1) has some amide protons (Gly28, Asp29, Ser34, Gly35, and Lys36) facing toward the solvent.

Other fast exchangeable HN protons, such as Gly48, Gly118, and Ala97, are located in the northern loops of the molecule. The other four amide protons (corresponding to residues Val56, Lys60, Asp73, and Tyr136) are in the β-barrel scaffold. It is interesting to remark that Val56 and Lys60 are close or in β-strand VI (see Table 1) that, in turn, is antiparallel aligned to the β-strand V. This substructure is a singular feature of Rc, and it is not present in the rest of BCPs (*27*). It is also noticeable that Tyr136 is buried to the solvent by the long loop encompassing residues 80−119. Hence, this loop is flexible enough to allow water molecules to interact with the β-strand X. The largest cross peak of the cleanex 2-D map corresponds to a side chain proton, specifically to Hϵ2 proton of His143, a copper ligand. This provides direct spectroscopic evidence of the degree of the solvent exposure of this imidazole group. In other BCPs, the analogous proton participates in electron auto-transfer via water molecules (*68*, *69*).

To determine the degree of the exposure of amide protons to the solvent over time scales longer than seconds, ^{15}N HSQC experiments on a fresh sample prepared in D_2O were collected from 3 h to two weeks after the H_2O/D_2O exchange. Forty-seven residues out of the 136 assigned HN groups (34.6%) do not appear in the experiment collected 3 h after the D_2O exchange ($R_{exch} > 10^{-4}$ s^{-1}). Fifty residues (36.7%) retain more than 50% of their initial intensity after 11 days ($R_{exch} < 10^{-6}$ s^{-1}). The remaining amino acids have an intermediate behavior (10^{-6} s^{-1} < R_{exch} < 10^{-4} s^{-1}). These results are schematically shown in Figure 3B. The 47 rapid exchanging residues (white color in Figure 3B) are located either at the beginning of the sequence, in the β-strand I, in the 26−37 region (which also involves β-strands II and III), or distributed over the loops connecting the strands of the β-barrel. The longest hydrophilic region corresponds to residues encompassing amino acids 93−130 (involving part of the long loop 79−119 and β-strand IX, see Table 1), which, at the same time, forms an antiparallel β-sheet with β-strand I. Forty out of the 50 slow exchanging residues (red color in Figure 3B) are mainly located in secondary structure elements characteristic of the classical BCP topology: 29 belong to the β-barrel structure; another three are located in the small α-helix region in the northern part of the molecule close to the copper site (Helix II, see Table 1); and eight are located in loops. The other 10 residues are placed in the N-terminal extension characteristic of Rc, situated at the end of the α-helix I and in the β-strands II and III (see Discussion).

Structural Water Molecules. Peaks observed in the ePHOGSY experiment (*52*, *53*) (data not shown) may arise from a direct NOE between protein groups and a water molecule trapped within the protein frame. However, as already described, other effects can contribute to ePHOGSY peaks in the absence of a real HN−water NOE (*37*, *39*). These are spin diffusion effects during the mixing time, the unwanted NOEs arising from Hα protons with the same chemical shifts of bulk water, and exchanged relayed NOEs. When all these effects have been properly taken into account (*39*), only Leu19 HN unambiguously arises from direct HN−water NOEs. This structural water molecule is found between α-helix I and the β-strands IV, and it is displayed (in green) in Figure 3A.

DISCUSSION

Dynamics and Hydration Properties of Rusticyanin versus other BCPs. The analysis of relaxation data clearly indicates a distinctive feature of Rc with regard to the other BCPs: its high rigidity.

In fact, Rc is the most rigid BCP. The average S^2 (0.93 ± 0.03) as well as the average NOE value (0.83 very close to the theoretical maximum, 0.835) indicate this feature of Rc. This suggests an unusually small degree of internal motion. This rigidity becomes more evident if we compare with the order parameters of Pc (0.87), Az (0.86), and PsAz (0.83). All these BCPs have a high S^2 value (i.e., a very fixed structure). This rigidity is caused by the protein scaffold imposed by the Greek key topology of the β-barrel and the high content in hydrogen bonds. This feature allows electron transfer with a low reorganization energy (*1*, *2*, *70*).

It has been argued that the unusual features of Rc are linked to its structural properties, and this is further reinforced by the finding reported here that Rc is considerably more rigid than other BCPs (*15*, *16*, *22*). An insight into the specific elements responsible for these properties can be gained if we analyze the dynamic properties of the region encompassing the residues 83−92 (inside the long loop connecting β-strands VIII and IX, Table 1). Although the secondary structure elements for the equivalent region are somewhat different from one BCP to another, its mobility features are analogous for the four studied BCPs (*40*−*42*). In fact, this domain has essentially similar values for the order parameter to those of the β-barrel regions (the S^2 average values are 0.93 and 0.94, respectively) (i.e., they are quite rigid even when no specific secondary structure elements are defined in this loop). Azurin, with an α-helix in this region (helix including residues 55−67 in Az, see Table 1) also shows high S^2 values (from 0.78 to 0.94) (*40*), although not as high as in Rc. In contrast, the degree of order in PsAz (*41*) (that lacks of a defined secondary structure for the equivalent residues) is lower than in Az and in Rc. Hence, not only secondary structure elements, but also tertiary interactions, are decisive in providing Rc its extraordinarily high rigidity.

A map of the exposition of amide protons to the solvent in Rc is displayed in Figure 3A,B. This map provides a clear picture of the second most characteristic feature of Rc: its high hydrophobicity. The 36.7% of Rc amide proton (50 out of 136) exchange very slowly ($R_{exch} < 10^{-6}$ s^{-1}) (i.e., they are hidden to the solvent). Analogous studies have only been performed in Pc (*42*). For this BCP, the nonexchangeable amide protons are reduced to 17.2% of the residues (16 out of 93 amide protons). The extension of the hydrophobic core in Rc may be partially due to the simple fact that this is a larger protein; hence, there exists a lower percentage of residues in the surface of the protein. However, there is a unique structural feature of Rc, the first 35 amino acids, that can also account for this high degree of hydrophobicity.

Distinctive Mobility Properties of the N-35 Terminal Extension. Rusticyanin possesses 35 amino acids extra, when compared to most other BCPs, that extends the N-terminus (*15*, *22*, *27*, *71*). This is comprised of the α-helix (helix I, Table 1) as well as by three β-strands (strands I, II, and III, Table 1), not present in the rest of BCPs.

The residue-by-residue analysis of our data, summarized in Figures 1 and 2, shows two regions with fast internal motions (in the nanosecond time scale): the N-terminal (first five amino acids) region and the loop within the amino acids 34−38. This last loop (which corresponds to the N-terminal region in the rest of BCPs, see Table 1) is then very flexible and seems to act as a linker between two regions. Both ccr and S^2 values show that the amino acids encompassing the two mobile regions (the N-terminal and the 34−38 regions) are quite rigid. Moreover, the amphipathic helix I seems to be (together with the C-terminal side) the most rigid part of the molecule. Thus, the region connecting the classic β-barrel to the first part of the molecule (amino acids 34−38) acts as if it couples two different modules: the specific module of Rc (the N-35 extension) and the rest of the protein (the typical BCP topology).

Crystallographic studies reveal that this extension acts as a belt with respect to the typical β-barrel fold (*16*, *19*, *26*). Given the peculiar features of Rc, this extension has been postulated to be the driving factor toward the increased acid stability of this protein. Nevertheless, an Rc mutant with the extension 1−35 deleted is still soluble in an acidic environment, being the N-terminal extension responsible for the shielding of the hydrophobic core (*27*). Our present findings corroborate this last point of view. The N-35 extension serves to increase the hydrophobic nature of the core of the typical β-barrel topology in Rc (*27*).

Relaxation NMR Data versus B-Factors Obtained from Crystallographic Structures. Temperature or *B*-factors in X-ray diffraction data are an indication about the degree of order (i.e., mobility) of each atom in the solid state. Tridimensional structures of Rc wild type (*16*) and some of its mutants (*19*, *26*) in the solid state have been reported. Thus, we can compare the *B*-factors of the amide nitrogen atoms in these structures with our present results. For doing this, we have chosen the two Rc structures deposited in the Protein Data Bank with the best degree of resolution (i.e., Met148Gln 1e30 (*19*) and Ser86Asp Rc mutants 1gy1 (*26*) resolved at 1.50 and 1.65 Å, respectively). In these two crystal structures, four regions have *B*-factors significantly larger than the average value. These are residues 35−37, 47−48, 69−70, and 116−119. The mobility observed in the present work for residues 35−37, 48 (47 is a proline), and 69−70 nicely agrees with X-ray data. Only partial agreement is found between NMR and X-ray data for residues 116−119. In fact, Lys119 has an R_1 value longer than the average (see Results), indicating the existence of fast motions for that amide backbone nitrogen, in agreement with crystal structure data. Cleanex experiment shows that Gly118 is exposed to the solvent and hence predisposed to exchange phenomena. Lys116 and Asp117 seem not to present fast mobility from our NMR data.

A further comment must be said about the *B*-factors in the N-terminal (residues 2−3) region. In the 1gy1 PDB file, Thr2 and Leu3 show very high *B*-values, while in the 1e30 PDB file, residue Leu3 has a temperature factor not excessively high. Our data for these two amino acids are clear and conclusive. While in the solid state, the N-terminal residues could be not mobile, in solution they decisively present mobility in the subnanosecond time scale.

Dynamic Features of the Copper Surroundings. Three of the copper ligands (Cys138, His143, and Met148) belong to

the last two final β-strands of Rc (Cys138 and Met148, see Table 1) or to the loop interconnecting both (His143). The last β-strand in Rc (β-strand XI) shows a very high S^2 order parameter (0.95). A similar pattern is observed for Pc(*42*), but Az(*40*) and PsAz(*41*) have mobile C-terminal extremes. Additionally, all the amide protons of this β-strand (except that of Met148) do not exchange with the solvent when the protein is dissolved in D_2O (Figure 3B). The antiparallel partner of β-strand XI, β-strand X, also shows a very similar pattern. Hence, these two β-strands form in Rc one of the most rigid and highly shielded (from solvent interaction) regions of the molecule. This could have two implications in the singular features of Rc. First, the greater protection of the backbone in this C-terminal region would provide an additional stabilizing effect, thus further guarding against denaturation of the protein. Second, the dynamic (and thus, the structural) properties of ligands Cys138 and Met148 (both belonging to these β-strands) will be determined by the interactions of these two β-strands, as we have already proposed (*72*). Therefore, it is possible that the high rigidity and hydrophobicity of the two antiparallel β-strands X and XI are, in some way, translated to the active center. A highly hydrophobic environment of the copper ion would increase the redox potential of the protein (*15*, *22*, *28*) and would be in agreement with the entatic or rack state mechanism for the copper ion (*1*, *73*). It would also explain the facility of the interconversion copper(I)/copper(II) (kinetics behavior). The other two ligands, histidines 85 and 143, also have a very high S^2 value (0.96 and 0.94, respectively), also indicating the high rigidity of the active center.

Cross relaxation rates in Cu(I) and Cu(II) Rc show no significant differences (see Results). Hence, the oxidation state of the metal ion does not alter the dynamic properties of Rc. This has been found previously in Pc (*42*). The opposite pattern has been found in other electron-transfer proteins such as cytochromes (*74*). As previously proposed (*72*), it is likely that the β-barrel scaffold in BCPs is a very high barrier for impeding the free mobility of the copper ion. This occurs in both oxidation states.

Dynamic Properties of Rc in the Millisecond Time Scale. Conformational exchange in the millisecond time scale has been observed in azurin for Gly37 (*40*). This was explained because of the acidic features of His35. This histidine is responsible for the small conformational change of the residues surrounding the metal ion, and as a consequence, the change of the redox potential of azurin with the pH. In PsAz, the equivalent amino acid to Gly37, Lys36, also shows conformational exchange in the same region (*41*), even when no histidine is present. The equivalent amino acid in Rc is Asn80. No mobility on the millisecond time scale is observed for this residue. In this region, only Thr79 presents fast mobility but in the nanosecond time scale. It is not clear whether this mobility is related to any conformational exchange phenomena analogous to that observed for Az and PsAz occurring on a slower time scale.

On the contrary, the most significant feature regarding motions in the millisecond time scale in Rc (Figures 1B and 2D) is the large exchange rates for residues His57 and Asp58 (16.2 and 25.7 Hz, respectively). This pattern can arise from the protonation/deprotonation behavior of the His57 imidazol ring at the working pH value. The implicated residues belong to the loop interconnecting the strands V and VI, not present in other BCPs. Interestingly, Val56 and Lys60 (belonging to the same loop) amide protons are in fast exchange with the solvent. It is likely that both exchange in the millisecond time scale and solvent exchange of this loop are related, although its physiological relevance (if it exists) cannot be deduced from the present study.

CONCLUSION

NMR studies on local dynamics and hydration of Rc contribute to a better understanding of the peculiar thermodynamic features of this protein. Rc has higher rigidity even than other BCPs. This holds not only within the β-barrel scaffold but also in the loop regions. This demonstrates that tertiary interactions are important in determining the dynamics of Rc. The degree of hydrophobicity of Rc is greater than in other BCPs. The N-35 extension, unique to Rc, plays an important role in shielding the β-barrel toward solvent exposure. These features are independent of the redox state of the metal ion. The body of experimental data presently available accounts for a direct relationship occurring between the average order parameter and the reduction potential of the protein. The present study represents an example of how protein dynamics links structure and function.

ACKNOWLEDGMENT

Drs. S. Samar Hasnain (CCLRC Daresbury Laboratory) and John F. Hall (De Monfort University) are acknowledged for providing us *E. coli* with the Rc plasmid, as well as for many interesting comments.

SUPPORTING INFORMATION AVAILABLE

The cleanex experiment. This material is available free of charge via the Internet at http://pubs.acs.org.

REFERENCES

1. Gray, H. B., Malmström, B. G., and Williams, R. J. P. (2000) Copper coordination in blue proteins, *JBIC 5*, 551−9.
2. Randall, D. W., Gamelin, D. R., LaCroix, L. B., and Solomon, E. I. (2000) Electronic Structure contributions to electron transfer in blue Cu and CuA, *JBIC 5*, 16−9.
3. Cox, J. C., Aasa, R., and Malmstrom, B. G. (1978) EPR studies on the blue copper protein, rusticyanin: a protein involved in Fe^{2+} oxidation at pH 2.0 in *Thiobacillus ferrooxidans*, *FEBS Lett. 93*, 157−60.
4. Shoham, M. (1992) Rusticyanin: Extremes in acid stability and redox potential explained by the crystal structure, *J. Mol. Biol. 227*, 581−2.
5. Ingledew, W. J., and Cocco, D. (1980) *Biochim. Biophys. Acta 590*, 141−58.
6. Blake, R. C., II, and Shute, E. A. (1987) Respiratory enzymes of *Thiobacillus ferrooxidans*. A kinetic study of electron transfer between iron and rusticyanin in sulfate media, *J. Biol. Chem. 262*, 14983−9.
7. Hall, J. F., Kanbi, L. D., Strange, R. W., and Hasnain, S. S. (1999) Role of the axial ligand in type 1 Cu centers studied by point mutations of Met148 in rusticyanin, *Biochemistry 38*, 12675−80.
8. Cobley, J. G., and Haddock, B. A. (1975) The respiratory chain of *Thiobacillus ferrooxidans*: the reduction of cytochromes by Fe^{2+} and the preliminary characterization of rusticyanin a novel blue copper protein, *FEBS Lett. 60*, 29−33.
9. Cox, J. C., and Boxer, D. H. (1978) The purification and some properties of rusticyanin, a blue copper protein involved in iron-(II) oxidation from *Thiobacillus ferrooxidans*, *Biochem. J. 174*, 497−502.
10. Hall, J. F., Hasnain, S. S., and Ingledew, W. J. (1996) The structural gene for rusticyanin from *Thiobacillus ferrooxidans*:

cloning and sequencing of the rusticyanin gene, *FEMS Microbiol. Lett. 137*, 85−9.
11. Ingledew, W. J., Cox, J. C., and Halling, P. J. (1977) A proposed mechanism for energy conservation during Fe^{2+} oxidation by *Thiobacillus ferrooxidans*: Chemiosmotic coupling to net H^+ influx, *FEMS Microbiol. Lett. 2*, 193−7.
12. Ronk, M., Shively, J. E., Shute, E. A., and Blake, R. C., II. (1991) Amino acid sequence of the blue copper protein rusticyanin from *Thiobacillus ferrooxidans*, *Biochemistry 30*, 9435−42.
13. Blake, R. C., II, Shute, E. A., Greenwood, M. M., Spencer, G. H., and Ingledew, W. J. (1993) Enzymes of aerobic respiration on iron, *FEMS Microbiol. Rev. 11*, 9−18.
14. Djebli, A., Proctor, P., Blake, R. C., II, and Shoham, M. (1992) Crystallization and preliminary X-ray crystallographic studies of rusticyanin from *Thiobacillus ferrooxidans*, *J. Mol. Biol. 227*, 581−2.
15. Grossmann, J. G., Ingledew, W. J., Harvey, I., Strange, R. W., and Hasnain, S. S. (1995) X-ray absorption studies and homology modeling define the structural features that specify the nature of the copper site in rusticyanin, *Biochemistry 34*, 8406−14.
16. Walter, R. L., Ealick, S. E., Friedman, A. M., Blake, R. C., II, Proctor, P., and Shoham, M. (1996) Multiple wavelength anomalous diffraction (MAD) crystal structure of rusticyanin: a highly oxidizing cupredoxin with extreme acid stability, *J. Mol. Biol. 263*, 730−51.
17. Harvey, I., Hao, Q., Duke, E. M., Ingledew, W. J., and Hasnain, S. S. (1998) Structure determination of a 16.8 kDa copper protein at 2.1 Å resolution using anomalous scattering data with direct methods, *Acta Crystallogr. D54*, 629−35.
18. Yu-dong, L., Harvey, I., Yuan-xin, G., Chao-de, Z., Yi-zong, H., Hai-fu, F., Hasnain, S. S., and Hao, Q. (1999) Is single-wavelength anomalous scattering sufficient for solving phases? A comparison of different methods for a 2.1 Å structure solution, *Acta Crystallogr. D55*, 1620−2.
19. Hough, M. A., Hall, J. F., Kanbi, L. D., and Hasnain, S. S. (2001) Structure of the M148Q mutant of rusticyanin at 1.5 Å: a model for the copper site of stellacyanin, *Acta Crystallogr. D57*, 355−60.
20. Hunt, A. H., Toy-Palmer, A., Cavanagh, J., Blake, R. C., II, and Dyson, H. J. (1994) Nuclear Magnetic Resonance Assignaments and Global Fold of Rusticyanin. Insights into the ligation and acid stability of the Blue Copper Site, *J. Mol. Biol 244*, 370−84.
21. Toy-Palmer, A., Prytulla, S., and Dyson, H. J. (1995) Complete ^{13}C assignments for recombinant Cu(I) rusticyanin. Prediction of secondary structure from patterns of chemical shifts, *FEBS Lett. 365*, 35−41.
22. Botuyan, M. A., Toy-Palmer, A., Chung, J., Blake, R. C., II, Beroza, P., Case, D. A., and Dyson, H. J. (1996) NMR Solution Structure of Cu(I) Rusticyanin from *Thiobacillus ferrooxidans:* Structural Basis for the Extreme Acid Stability and Redox Potential, *J. Mol. Biol. 263*, 752−67.
23. Holt, S. D., Piggott, B., Ingledew, W. J., Feiters, M. C., and Diakun, G. P. (1990) EXAFS of the type 1 copper site of rusticyanin, *FEBS Lett. 269*, 117−21.
24. Nunzi, F., Guerlesquin, F., Shepard, W., Guigliarelli, B., and Bruschi, M. (1994) Active site geometry in the high oxido-reduction potential rusticyanin from *Thiobacillus ferrooxidans*, *Biochem. Biophys. Res. Commun. 203*, 1655−62.
25. Hall, J. F., Kanbi, L. D., Harvey, I., Murphy, L. M. M., and Hasnain, S. S. (1998) Modulating the Redox Potential and Acid Stability of Rusticyanin by Site-Directed Mutagenesis of Ser86, *Biochemistry 37*, 11451−8.
26. Kanbi, L. D., Antonyuk, S., Hough, M. A., Hall, J. F., Dodd, F. E., and Hasnain, S. S. (2002) Crystal Structures of the Met148Leu and Ser86Asp Mutants of Rusticyanin from *Thiobacillus ferrooxidans*: Insights into the Structural Relationship with the Cupredoxins and the Multi Copper Proteins, *J. Mol. Biol. 320*, 263−75.
27. Grossmann, J. G., Hall, J. F., Kanbi, L. D., and Hasnain, S. S. (2002) The N-terminal extension of rusticyanin is not responsible for its acid stability, *Biochemistry 41*, 3613−9.
28. Donaire, A., Jiménez, B., Moratal, J. M., Hall, J. F., and Hasnain, S. S. (2001) Electronic Characterization of the Oxidized State of the Blue Copper Protein Rusticyanin by ^1H NMR: Is the Axial Methionine the Dominant Influence for the High Redox Potential? *Biochemistry 40*, 837−46.
29. Palmer, A. G., III. (2001) NMR probes of molecular dynamics: overview and comparison with other techniques, *Annu. Rev. Biophys. Biomol. Struct. 30*, 129−55.
30. Dayie, K. T., Wagner, G., and Lefevre, J. F. (1996) Theory and practice of nuclear spin relaxation in proteins, *Annu. Rev. Phys. Chem. 47*, 243−82.
31. Peng, J. W., and Wagner, G. (1994) Investigation of protein motions via relaxation measurements, *Methods Enzymol. 239*, 563−96.
32. Palmer, A. G., III, Kroenke, C. D., and Loria, J. P. (2001) Nuclear magnetic resonance methods for quantifying microsecond-to-millisecond motions in biological macromolecules, *Methods Enzymol. 339*, 204−38.
33. Bax, A. (2003) Weak alignment offers new NMR opportunities to study protein structure and dynamics, *Protein Sci. 12*, 1−16.
34. Brunne, R. M., Lieppinsh, E., Otting, F., Wüthrich, K., and van Gunsteren, W. F. (1993) Hydration of Proteins. A Comparison of Experimental residence times of Water Molecules Solvating the Bovine Pancreatic Trypsin Inhibitor with Theoretical Model Calculation, *J. Mol. Biol. 231*, 1040−8.
35. Otting, G., and Lieppinsh, E. (1995) Protein Hydration viewed by high-resolution NMR Spectroscopy: implications for Magnetic Resonance Image Contrast, *Acc. Chem. Res. 28*, 171−7.
36. Wider, G. (1998) Technical aspects of NMR spectroscopy with biological macromolecules and studies of hydration in solution, *Prog. NMR Spectrosc. 32*, 193−275.
37. Bertini, I., Dalvit, C., Luchinat, C., Huber, J. G., and Piccioli, M. (1997) e-PHOGSY Experiments on a paramagnetic protein: location of the catalytic water molecule in the heme crevice of the oxidized form of Horse Heart Cytochrome *c*, *FEBS Lett. 415*, 45−8.
38. Mesgarzadeh, A., Pfeiffer, S., Engelke, J., Lassen, D., and Ruterjans, H. (1998) Bound water in apo and holo bovine heart fatty-acid-binding protein determined by heteronuclear NMR spectroscopy, *Eur. J. Biochem. 251*, 781−6.
39. Bertini, I., Huber, J. G., Luchinat, C., and Piccioli, M. (2000) Protein hydration and location of water molecules in oxidized horse heart cytochrome *c* by ^1H NMR, *J. Magn. Reson. 147*, 1−8.
40. Kalverda, A. P., Ubbink, M., Gilardi, G., Wijmenga, S. S., Crawford, A., Jeuken, L. J., and Canters, G. W. (1999) Backbone dynamics of azurin in solution: slow conformational change associated with deprotonation of histidine 35, *Biochemistry 38*, 12690−7.
41. Thompson, G. S., Leung, Y. C., Ferguson, S. J., Radford, S. E., and Redfield, C. (2000) The structure and dynamics in solution of Cu(I) pseudoazurin from *Paracoccus pantotrophus*, *Protein Sci. 9*, 846−58.
42. Bertini, I., Bryant, D. A., Ciurli, S., Dikiy, A., Fernandez, C. O., Luchinat, C., Safarov, N., Vila, A. J., and Zhao, J. (2001) Backbone dynamics of plastocyanin in both oxidation states. Solution structure of the reduced form and comparison with the oxidized state, *J. Biol. Chem. 276*, 47217−26.
43. Bodenhausen, G., and Ruben, D. J. (1980) Natural abundance nitrogen-15 NMR by enhanced heteronuclear spectroscopy, *Chem. Phys. Lett. 69*, 185−9.
44. Kozmisnki, W. (1999) Simplified Multiplet pattern HSQc-TOCSY experiment for accurate determination of long-range heteronuclear coupling constants, *J. Magn. Reson. 137*, 408−12.
45. Kay, L. E., Ikura, M., Tschudin, R., and Bax, A. (1990) Three-Dimensional Triple-Resonance NMR Spectroscopy of Isotopically Enriched Proteins, *J. Magn. Reson. 89*, 496−514.
46. Farmer, B. T., II, Venters, R. A., Spicer, L. D., Wittekind, M. G., and Müller, L. (1992) A refocused and optimized HNCA: increased sensitivity and resolution in large macromolecules, *J. Biomol. NMR 2*, 195−202.
47. Kay, L. E., Nicholson, L. K., Delaglio, F., Bax, A., and Torchia, D. A. (1992) Pulse sequences for removal of the effects of cross correlation between dipolar and chemical-shift anisotropyrelaxation mechanisms on the measurement of heteronuclear T1 and T2 values in proteins, *J. Magn. Reson. 97*, 359−75.
48. Grzesiek, S., and Bax, A. (1993) The importance of not saturating water in protein NMR. Application to sensitivity enhancement and NOE measurements, *J. Am. Chem. Soc. 115*, 12593−4.
49. Sklenar, V., and Bax, A. (1987) Spin−Echo Water Supression for the Generation of Pure-Phase Two-Dimensional NMR Spectra, *J. Magn. Reson. 74*, 469−79.
50. Tjandra, N., Szabo, A., and Bax, A. (1996) Protein Backbone Dynamics and ^{15}N Chemical Shift Anisotropy from Quantitative Measurement of Relaxation Interference Effects, *J. Am. Chem. Soc. 118*, 6986−91.
51. Hwang, T.-L., van Zijl, P. C. M., and Mori, S. (1998) Accurate quantitation of water−amide proton exchange rates using the

phase-modulated CLEAN chemical EXchange (CLEANEX-PM) approach with a Fast-HSQC (FHSQC) detection exchange, *J. Biomol. NMR 11*, 221−6.
52. Dalvit, C. (1996) Homonuclear 1- and 2-D NMR experiments for the observation of solvent−solute interactions, *J. Magn. Reson. Ser. B 112*, 282−8.
53. Dalvit, C., and Hommel, U. (1995) Sensitivity-improved detection of protein hydration and its extension to the assignment of fast-exchanging resonances, *J. Magn. Reson. Ser. B 109*, 334−8.
54. Marquardt, D. W. (1963) An Algorithm for least squares estimation of nonlinear parameters, *J. Soc. Ind. Appl. Math. 11*, 431−41.
55. Press, W. H., Flannery, B. P., Teukolsky, S. A., and Vetterling, W. T. (1988) *Numerical Recipes in C: The Art of Scientific Computing*, Cambridge University Press, New York.
56. Peng, J. W., and Wagner, G. (1992) Mapping of the spectral densities of nitrogen−hydrogen bond motions in Eglin *c* using heteronuclear relaxation experiments, *Biochemistry 31*, 8571−86.
57. Palmer, A. G., III, Rance, M., and Wright, J. G. (1991) Intramolecular motions of a zinc finger DNA-binding domain from Xfin characterized by proton-detected natural abundance carbon-13 heteronuclear NMR spectroscopy, *J. Am. Chem. Soc. 113*, 4371−80.
58. Lee, L. K., Rance, M., Chazin, W. J., and Palmer, A. G., III. (1997) Rotational diffusion anisotropy of proteins from simultaneous analysis of ^{15}N and ^{13}C α nuclear spin relaxation, *J. Biomol. NMR 9*, 287−98.
59. Tjandra, N., Kuboniwa, H., Ren, H., and Bax, A. (1995) Rotational dynamics of calcium-free calmodulin studied by ^{15}N NMR relaxation measurements, *Eur. J. Biochem. 230*, 1014−24.
60. Mandel, A. M., Akke, M., and Palmer, A. G., III. (1995) Backbone dynamics of *Escherichia coli* ribonuclease HI: correlations with structure and function in an active enzyme, *J. Mol. Biol. 246*, 144−63.
61. Devore, J. (1982) *Probability and Statistics for Engineering and the Sciences*, Brooks/Cole Publishing Company, Monterey, CA.
62. Bevington, P. R., and Robinson, D. K. (1992) *Data Reduction and Error Analysis for the Physical Sciences*, McGraw-Hill, Inc., New York.
63. Lipari, G., and Szabo, A. (1982) Model-Free Approach to the interpretation of Nuclear Magnetic Resonance Relaxation in Macromolecules. 1. Analysis of Experimental Results, *J. Am. Chem. Soc. 104*, 4559−70.
64. Lipari, G., and Szabo, A. (1982) Model-Free Approach to the interpretation of Nuclear Magnetic Resonance Relaxation in Macromolecules. 1. Theory and Range of Validity, *J. Am. Chem. Soc. 104*, 4546−59.
65. Kay, L. E., Torchia, D. A., and Bax, A. (1989) Backbone dynamics of proteins as studied by nitrogen-15 inverse detected heteronuclear NMR spectroscopy: application to staphylococcal nuclease, *Biochemistry 28*, 8972−9.
66. Zinn-Justin, S., Berthault, P., Guenneugues, M., and Desvaux, H. (1997) Off-resonance RF fields in heteronuclear NMR. Application to the study of slow motions, *J. Biomol. NMR 10*, 363−72.
67. Fushman, D., and Cowburn, D. (2001) in *Methods in enzymology* (James, T. L., Dötsch, V., and Schmitz, U., Eds.) pp 109−26, Academic Press, San Francisco, CA.
68. Groeneveld, M., Ouwerling, M. C., Erkelens, C., and Canters, G. W. (1988) ^{1}H Nuclear magnetic resonance study of the protonation behavior of the histidine residues and the electron self-exchange reaction of azurin from *Alcaligenes denitrificans*, *J. Mol. Biol. 200*, 189−99.
69. Moratal Mascarell, J. M., Salgado, J., Donaire, A., Jimenez, H. R., and Castells, J. (1993) 1- and 2-D NMR Studies of the pH Effects on the metal-site geometry in Nickel(II) Azurin from *Pseudomonas aeruginosa*, *J. Chem. Soc., Chem. Commun.* 110−2.
70. Langen, R., Colon, J. L., Casimiro, D. R., Karpishin, J. R., Winkler, J. R., and Gray, H. B. (1996) Electron tunnelling in proteins. Role of the intervening medium, *JBIC 1*, 221−5.
71. Nunzi, F., Woudstra, M., Campese, D., Bonicel, J., Morin, D., and Bruschi, M. (1993) Amino acid sequence of rusticyanin from *Thiobacillus ferrooxidans* and its comparison with other blue copper proteins, *Biochim. Biophys. Acta 1162*, 28−34.
72. Donaire, A., Jiménez, B., Fernández, C. O., Pierattelli, R., Niizeki, T., Moratal, J. M., Hall, J. F., Kohzuma, T., Hasnain, S. S., and Vila, A. J. (2002) Metal−Ligand Interplay in Blue Copper Proteins Studied by ^{1}H NMR Spectroscopy: Cu(II)-Pseudoazurin and Cu(II)-Rusticyanin, *J. Am. Chem. Soc. 124*, 13698−708.
73. Malmström, B. G. (1994) Rack-induced bonding in blue copper proteins, *Eur. J. Biochem. 233*, 711−8.
74. Barker, P. B., Bertini, I., Del Conte, R., Ferguson, D. M., Hajieva, P., Tomlinson, E., Turano, P., and Viezzoli, M. S. (2001) A further clue to understanding the mobility of mitochondrial yeast cytochrome *c*: a ^{15}N T1rho investigation of the oxidized and reduced species, *Eur. J. Biochem. 268*, 4468−76.

BI034692Q